The Pennsylvania State University

DE-FG07-01ID14115

(DOE-NEER Project)

Report for Phase III and Final Project Report

Irradiation Induced Precipitation and Dissolution of
Intermetallics in Zr alloys studied using Synchrotron Radiation.

P.I.: Arthur T. Motta, The Pennsylvania State University

Report Period: Overall Project Period (August 16, 2001 to August 15, 2004) with emphasis on Phase III (August 16, 2003 to August 15, 2004)

Table of Contents

1. Summary

We present here the progress report for Phase III and the Final Report for the project above. The overall aim of this project is to investigate the irradiation induced precipitation of alloying elements and dissolution of second phase particles in Zr alloys using a combination of (i) synchrotron radiation examination of bulk samples using the Advanced Photon Source (APS) at Argonne National Laboratory and (ii) in-situ irradiation of model alloys using the IVEM/Tandem Facility also located at Argonne.

During the project period, we accomplished the majority of the tasks we set out to do. Because of the unavailability of the hot cells at Argonne National Laboratory, which had to undergo renovation during the period of the research, we were not able to perform the task related to the examination of neutron irradiated samples. Instead we created a procedure for investigating irradiation induced precipitation using model alloys in thin films. Such a procedure also proved useful to studying grain growth under irradiation. We also developed techniques that allow the characterization of bulk precipitate microstructure so that modifications induced by irradiation can be detected more precisely. The research has already yielded publications and more will be forthcoming, as shown in the references section. One Ph.D. student in Nuclear Engineering, Djamel Kaoumi, and one M.Sc. student in Materials, Sarah Jurgensmeier, performed their graduate work at Penn State while funded by this research project.

2. Examination of Thermal Precipitation using Synchrotron Radiation Diffraction

Participants: Sarah Jurgensmeier (M.Sc. student at Penn State) and Dr. Yong Chu (Argonne National Laboratory)

By utilizing the facilities at APS, we were able to increase the resolution and precision of XRD data collected, as compared with conventional sources, and so to identify additional phases present in model alloys. The sensitivity of the results is greater than those from previous examinations due in large part to the greater resolution capabilities at the APS. Such data will help the modeling of the behavior of these alloys in service, as the specific roles of precipitates and alloying elements in solution in affecting microstructural evolution under irradiation can be distinguished. During the project, we performed x-ray diffraction data on model alloys obtained from Cézus, France, and which were characterized otherwise by TEM. These model alloys were designed to have different Fe/Cr ratios, and as a result their precipitation behavior changed also. We review the results in the sections below.

The x-ray diffraction data was acquired by examining the samples in theta-two theta geometry using a step size of .002 degrees two theta for the range of 18 to 45 degrees (figure 1). The time counted per point was not set, but, instead, the count continued until the total photon count at each point reached a fixed value (250000 to 1 million counts, thus achieving good statistics). A standard NIST line positioning standard silicon powder number 640C was tested to ensure the accuracy of the setup. The data was fitted using two approaches: Rietveld refinement of the full profile using GSAS and manual fitting of the profile using PeakFit v.4.0. Figure 2 is the graphical output returned from a GSAS fit of a x-ray diffraction pattern from Zircaloy-4. The top spectrum is an overlay of the raw data with the generated fit. The bottom line is the residual showing the difference between the

experimental and calculated values. As is apparent, there is a large difference between the two, due mainly to the difficulty in refining the strong texture exhibited by the zirconium matrix in these alloys. Because of such difficulties, further analysis depended more heavily on the manual fitting method described below than on Rietveld refinement.

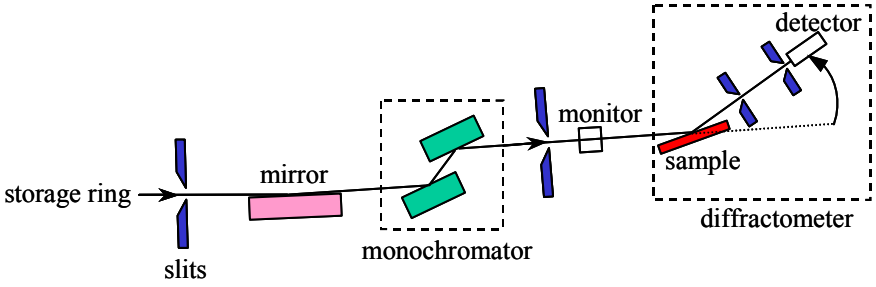

Figure 1: Experimental setup at Advanced Photon Source.

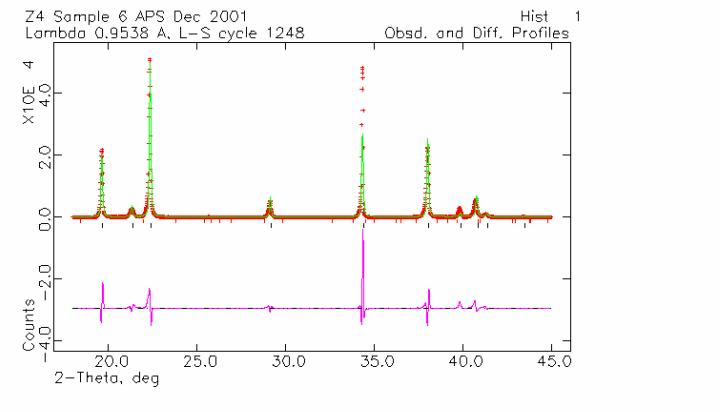

Figure 2*:* GSAS Graphical Output: actual data overlaid with fit and residuals for Zircaloy-4 CAP=5x10^{-18} h.

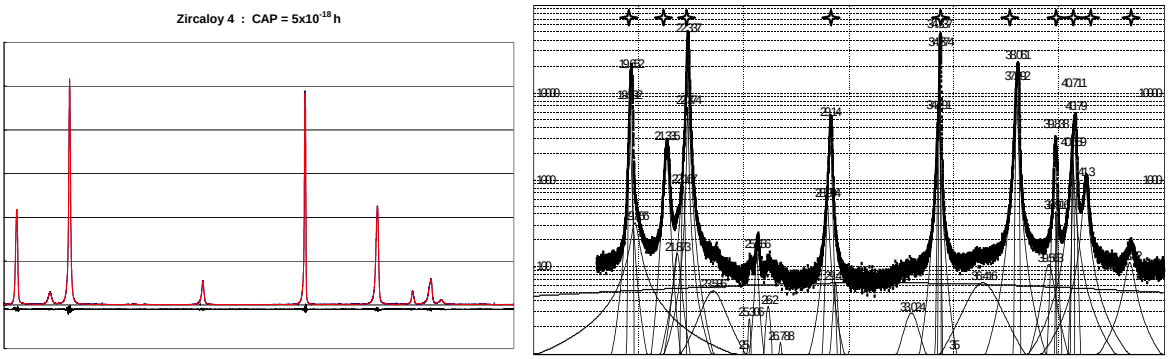

Figure 3: *(a)* Example Peak Fit 4.0 fit with residuals, intensity (linear scale) versus two theta angle. *(b)* Individual peaks used in the fitting.

The same x-ray diffraction pattern is shown in Figure 3a, fitted manually using PeakFit.

It shows the fitted line, and, below, the residuals for the fit (difference between fitted line and actual data) for a Zircaloy-4 sample. Because of the linear intensity scale, the second phase particle peaks are not clearly visible. These are more easily visible in Fig.3b (in the 2q range 25-27 degrees). The r-squared value of this fit was .9997. The residuals are on the magnitude of +/- 1000 counts where the highest peak intensity is above 50,000 counts, resulting in less than a two percent error .

These methods were used to examine two series of samples: ZrFeCr model alloys series and ZrCrNi model alloy series.

2.1 ZrFeCr Model alloys

The ZrFeCr model alloys were examined in two different states (i) quenched and heat-treated for one hour at 600 C and (ii) for 50 h at 750 C. We divide the presentation of the results by Fe/Cr ratio.

2.1.1. Fe/Cr ratio ≈ 1

For this series of samples there were two total alloying element content used, that is, totals of approximately 1% and 0.2%, but keeping the ratio of Fe/Cr ratio approximately equal to 1.

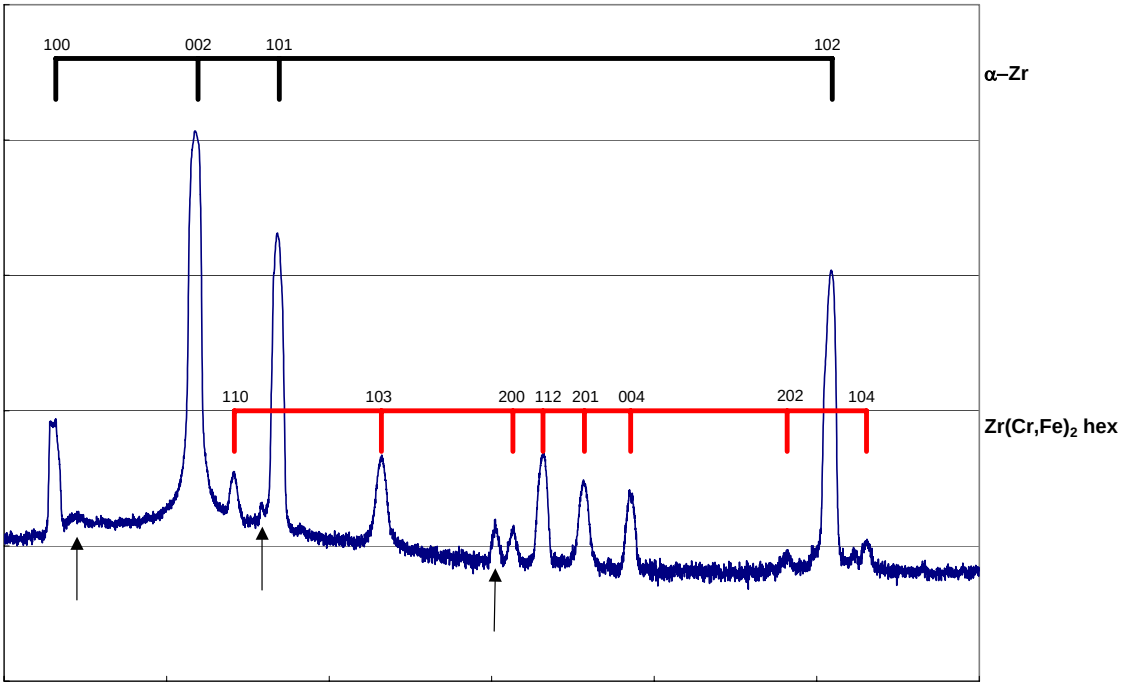

Figure 4: Phase indexing of diffraction pattern obtained for model alloy 0.45 Fe 0.435 Cr (total ~ 0.9%) heat treated for 50 hours at 750 °C (log scale).

Figure 4 shows the diffraction pattern from the sample with Fe/Cr ratio = 1 and total alloying content =0.9%, after anneal at 750 C for 50 h. The $Zr(Cr,Fe)_2$ hexagonal C14 phase is identified as being the

crystal structure of the main second phase present because the $Zr(Cr,Fe)_2$ hexagonal showing the peak locations allows to account for all the minor peaks (those not belonging to alpha Zr). In the previous annealing state the same hexagonal form of the $Zr(Cr,Fe)_2$ precipitate is seen, (figure 5) but with broader and lower peaks, indicating the presence of particles that are smaller and possibly under greater stress after the short annealing.

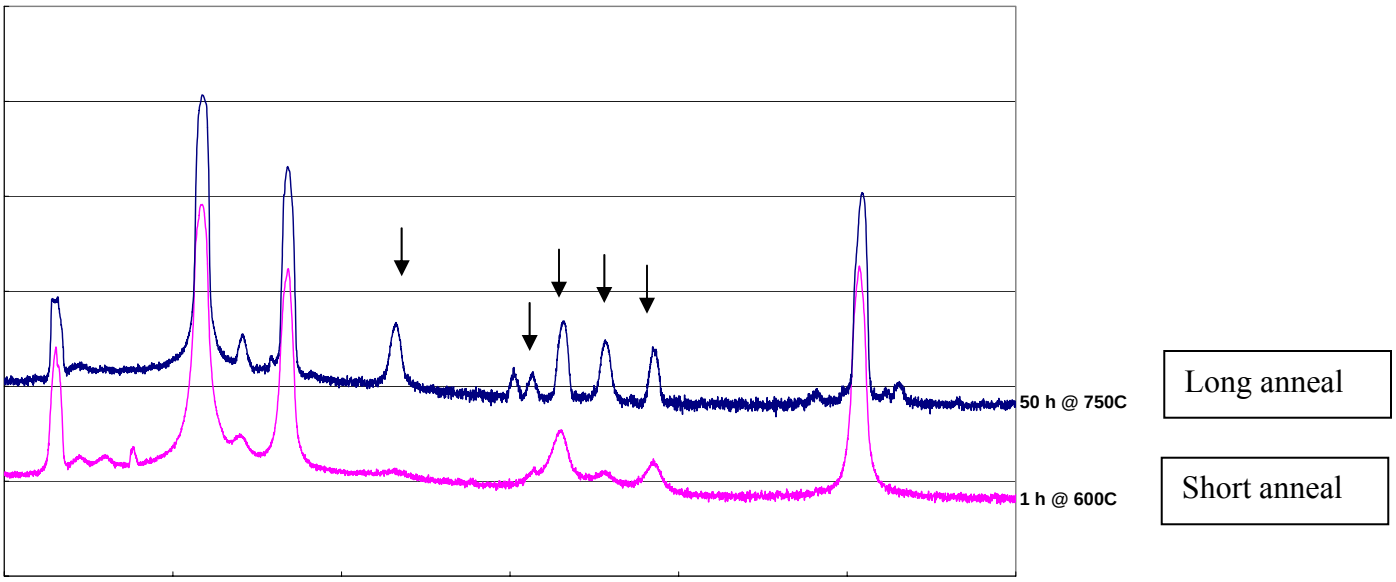

Figure 5: Evolution of 0.45 Fe 0.435 Cr Model Alloy with Heat Treatment Arrows indicate $Zr(Cr,Fe)_2$ peaks.

2.1.2. Fe/Cr ratio = 4

For this series, a sample was used that had a total alloying element content of approximately 0.2%. The results are shown in Figure 6. The indexing for the x-ray diffraction pattern obtained for the sample annealed at 600 C for 1 h are consistent with a mixture of hexagonal C14 $Zr(Cr,Fe)_2$, cubic $Zr(Cr,Fe)_2$ and orthorrombic Zr_3Fe, while the x-ray diffraction pattern obtained for the sample annealed at 750 C for 50 h shows evidence only of $Zr(Cr,Fe)_2$ in hexagonal form (mostly) and cubic (smaller amount). This indicates that the Zr_3Fe phase appears in richer Fe samples, as normally expected, but it is unstable and transforms to the more stable $Zr(Cr,Fe)_2$. The hexagonal and cubic variants have a comparatively small difference in free energy so that both forms of the $Zr(Cr,Fe)_2$ precipitate are still present after the long anneal, but a trend towards decreasing amounts of cubic $Zr(Cr,Fe)_2$ at higher annealing schedules was identified.

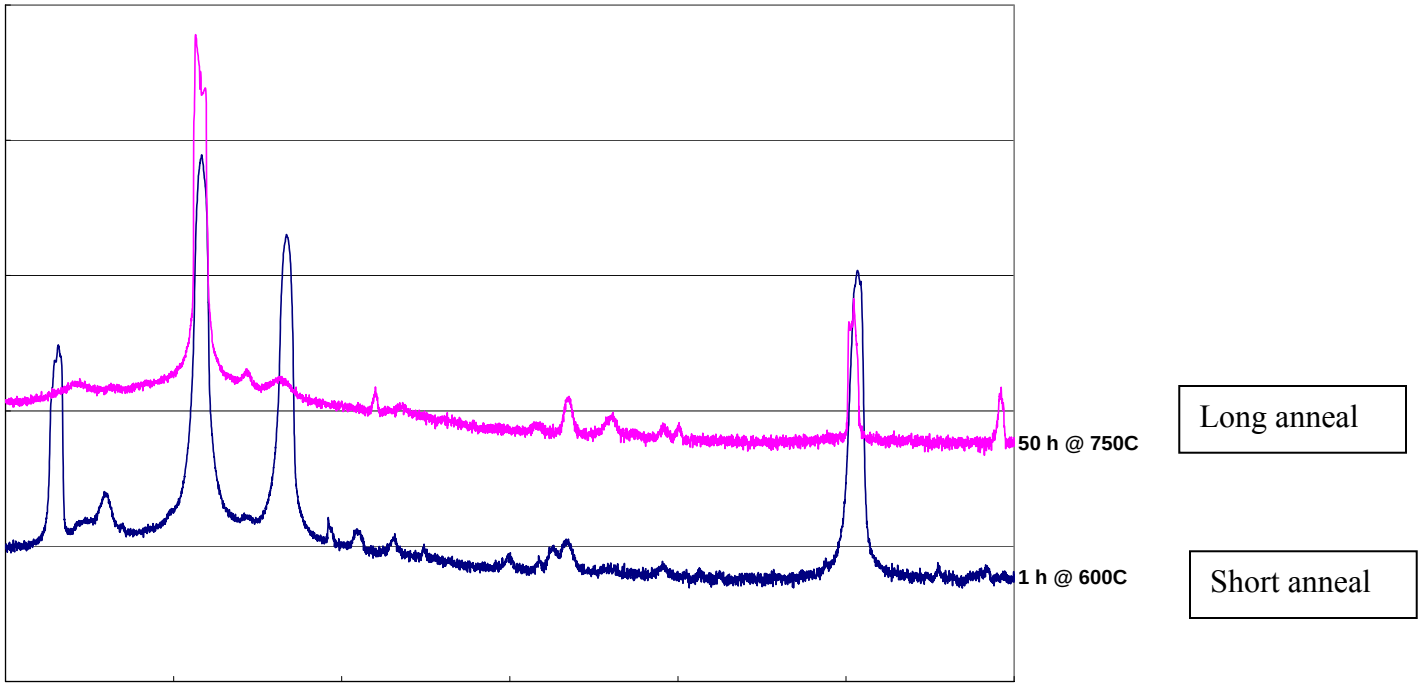

Figure 6: Evolution of 0.16 Fe 0.04 Cr Model Alloys (Fe/Cr~4) with Heat Treatment

2.1.3. Fe/Cr ratio= 1/4

For these samples, a total alloying element content of 0.2% was used. The phases identified were again cubic and hexagonal $Zr(Cr,Fe)_2$ but with the particularity that in the lower annealing schedule samples the hexagonal phase showed quite broad peaks, indicating small particle size while the cubic phase tended to be quite sharp, indicating larger precipitates. The greater content and larger size of the hexagonal precipitate relative to cubic $Zr(Cr,Fe)_2$ is expected from thermodynamic stability considerations. This is because as the Fe content decreases, the cubic phase becomes favored over the hexagonal phase. Thus the picture is that hexagonal precipitates initially form, likely because the Fe moves faster than Cr and the initial small precipitates are enriched in Fe. As the Cr arrives into the precipitates the balance shifts towards more stable cubic precipitates of the $ZrCr_2$ type.

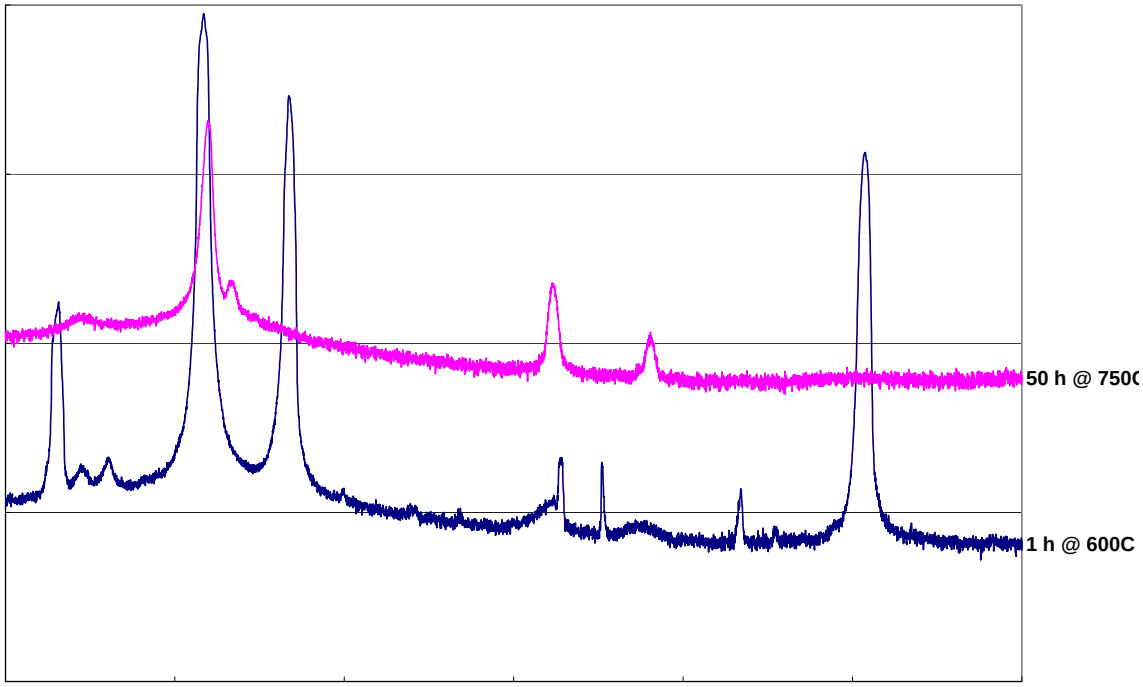

Figure 7: Evolution of 0.04 Fe 0.16 Cr (Fe/Cr ~1/4) Model Alloys with Heat Treatment.

2.2. ZrCrNi Alloys

This alloy examined had a total alloying content of ~ 1% (Cr+Ni). The x-ray diffraction pattern obtained showed evidence for body centered tetragonal C16 Zr_2Ni precipitates and cubic C15 $ZrCr_2$ precipitates. These are the thermodynamically expected phases, since when $ZrCr_2$ has low Fe/Cr ratio the cubic phase is the most stable.

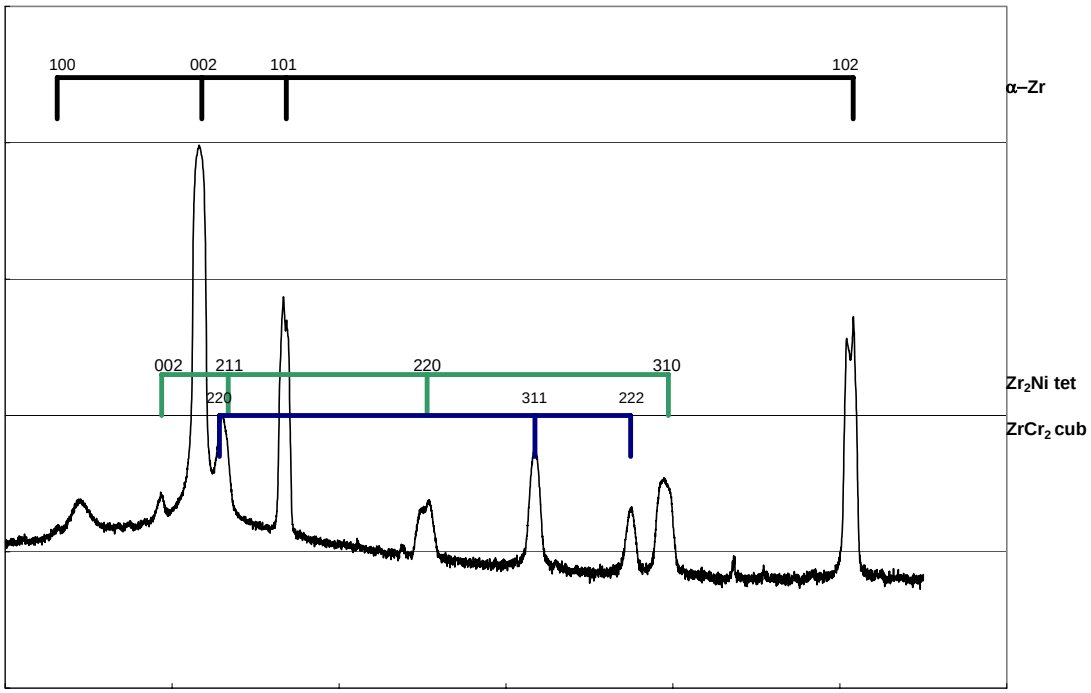

Figure 8. Phase indexing of diffraction pattern obtained for model alloy 0.472 Cr 0.502 Ni heat treated for 50 hours at 750 °C.

Analysis of these experiments has yielded the variation of precipitate content, lattice parameter and precipitate size with annealing as described in the following.

2.3. Analysis of results

The manual fitting of the profiles followed by a least squares optimization of the lattice parameter to reproduce the observed peak locations yields the lattice parameters for each phase shown in Table 1. Except for the values measured for the first alloy (which refers small precipitates formed during a short anneal) the values of the lattice parameters are quite consistent with each other. There is however, a slight trend in the lattice parameters (values of a and c in the hexagonal $Zr(Cr,Fe)_2$ structure) with increasing Cr content, as shown in Figures 9 and 10. Figure 9 shows the value of the lattice parameter "a" determined for various Fe/Cr ratios in this work (squares) and plotted against other values in the literature and determined by other techniques. Figure 10 shows the analogous plot for the "c" lattice parameter. The agreement is quite good indicating that this experimental method is a powerful way of investigating the precipitate microstructure in bulk alloys.

Phase Description	Fe/Cr Ratio	$Zr(Cr,Fe)_2$ hex a (Å)	$Zr(Cr,Fe)_2$ hex c (Å)	$Zr(Cr,Fe)_2$ cub a (Å)
0.045 Fe 0.150 Cr 1h@600°C	0.3	5.148	8.463	7.209
0.450 Fe 0.435 Cr 1h@600°C	1.03	5.036	8.262	N/A
0.155 Fe 0.043 Cr 1h@600°C	3.6	5.0194	8.225	7.118
0.045 Fe 0.150 Cr 50h@750°C	0.3	N/A	N/A	7.178
0.103 Fe 0.095 Cr 50h@750°C	1.08	5.038	8.262	N/A
0.450 Fe 0.435 Cr 50h@750°C	1.03	5.0363	8.258	N/A
0.155 Fe 0.043 Cr 50h@750°C	3.6	5.025	8.218	7.115

Table 1: Calculated Lattice parameters for the phases studied in this work

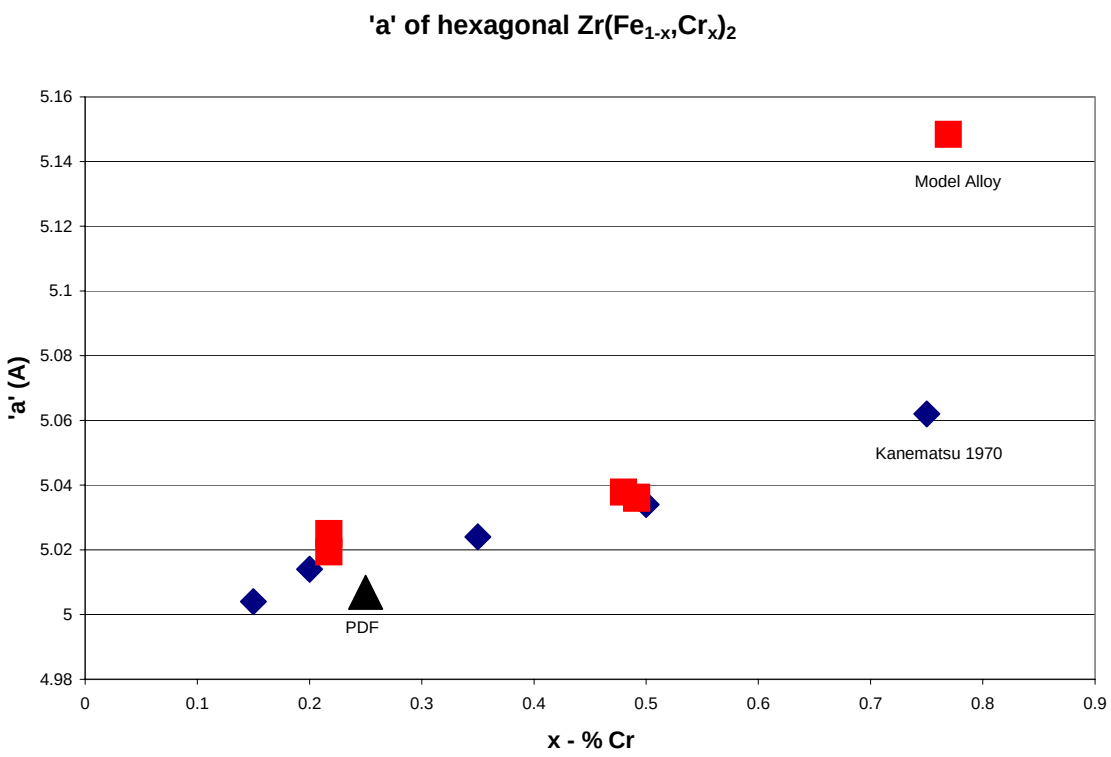

Figure 9: Lattice parameter "a" in the $Zr(Cr,Fe)_2$ crystal structure versus Cr content (squares are from this work, blue diamonds from Kanematsu [J.Phys.Soc.Jpn, 31(5) 1971, 1355-1360] and the black triangle the standard powder diffraction file for this compound)

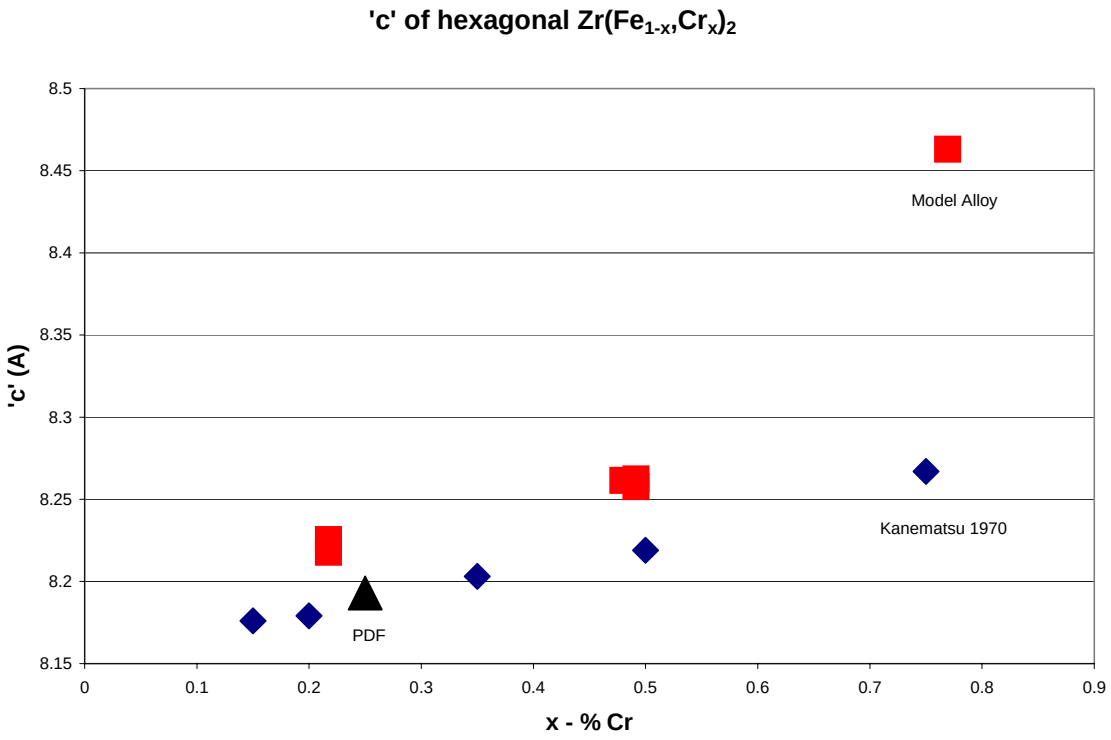

Figure 10: Lattice parameter "c" in the $Zr(Cr,Fe)_2$ crystal structure versus Cr content (squares are from this work, blue diamonds from Kanematsu [J.Phys.Soc.Jpn, 31(5) 1971, 1355-1360] and the black triangle the standard powder diffraction file for this compound)

	$Zr(Fe,Cr)_2$ Hexagonal	$ZrCr_2$ Cubic	Zr_3Fe Orthorhombic	Zr_2Fe Cubic
0.450 Fe 0.435 Cr 1 h 600°C	60 nm 110, 220, 112, 201, 004			
0.155 Fe 0.043 Cr 1 h 600°C	79.5 nm 103, 201		155 nm 040, 131, 060	67.5 nm 220, 311, 222
0.045 Fe 0.015 Cr 1 h 600°C	239.5 nm 103, 201, 004	52.2 nm 222		
0.103 Fe 0.095 Cr 50h 750°C	89.5 nm 110, 103, 200, 112, 201, 004			
0.450 Fe 0.435 Cr 50 h 750°C	112 nm 110, 103, 200, 112, 201, 004, 202, 104			
0.155 Fe 0.043 Cr 50 h 750°C	104 nm 103, 200, 201			92 nm 220, 311, 222
0.045 Fe 0.015 Cr 50 h 750°C		107 nm 311, 222		

Table 2: Particle size for the ZrCrFe Model Alloys. Each entry contains the average particle size, in nm, and then list the indices of the peaks used to compute the average particle size.

The particle size of the precipitates studied could be determined using the Debye Scherrer formula

$$d = \frac{0.9\,\lambda}{B_\theta \cos\theta}$$

where $B_\theta = (B^2 - B_i^2)^{1/2}$ is the particle size broadening for peak θ, B is the measured peak broadening (full-width half maximum, FWHM), B_i is the instrumental broadening measured using a standard, θ is the diffraction angle and λ is the wavelength of the synchrotron radiation. Using a pattern measured from a LaB_6 standard obtained from NIST we determined the instrumental broadening in this case to be 0.039 degrees two-theta. This technique for measuring particle size is useful in the range 0-100 nm, which coincidentally is the range of greater interest for the present experiments, as the precipitate size when fully annealed is on the order of 100-200 nm.

This was done for all the phases studied in this work and the results are shown in Table 2.

3. In-situ Irradiation Microstructure evolution in Zr-Fe Alloys (in collaboration with Dr. Robert Birtcher (MSD/Argonne National Laboratory)

3.1 Experimental Procedure

In this section of the research program, we have studied a very important problem of irradiation-induced microstructural evolution in Zr alloys, namely, the irradiation induced precipitation and dissolution of second phases. This is important, because the distribution of these alloying elements, in precipitates or in solution in the Zr matrix determines fuel cladding behavior at high burnup. The overall objective of these examinations is to understand, quantify and model the overall behavior of alloying elements such as Fe, Cr and Ni in nuclear fuel cladding under irradiation.

We have subjected free-standing thin films of Zr that were supersaturated with Fe at Argonne National Laboratory to irradiation by various ions at a range of temperatures to understand the kinetics of precipitation and dissolution of these second phases under irradiation. The thin films contain Fe concentrations that are above the thermodynamic solid solubility; however, because of the rapidity of the effective quench during thin film deposition the second phases do not form and these films are formed as supersaturated solid solutions. We have begun to quantify, using electron diffraction the appearance of second-phase precipitates in these alloys when they are subjected to ion irradiation and contrast these with the purely thermal reaction. We have performed these irradiations in-situ using the Intermediate Voltage Electron Microscope at Argonne.

Table 3 shows the in-situ experiments conducted in this project:

Table 3: List of experiments conducted at the IVEM facility at Argonne.

Fe content in the Zr-Fe samples	**Ion type/ Energy**	**Temperature °K (max fluence reached in ions/cm^2)**
0% Fe	Kr 500 keV	20 (10^{16}); 298 (10^{16})
1.2% Fe	Thermal run (no irradiation)	[298 – 823]
	Ar 500 keV	50 ($1.5\ 10^{16}$)
	Ar 600 keV	498($1.25\ 10^{16}$); 573($1.2\ 10^{16}$)
	Kr 500 keV	20 (10^{16}); 50 ($1.5\ 10^{16}$); 573 (10^{16}), 623 ($7.5\ 10^{15}$)
	Kr 600 keV	298 ($1.5\ 10^{16}$); 423 ($1.5\ 10^{16}$), 498 ($1.5\ 10^{16}$), 573 (10^{16}), 623(10^{16})
2% Fe (nominal composition)	Ar 500 keV	50K ($2\ 10^{16}$); 298 ($1.5\ 10^{16}$); 423 ($1.5\ 10^{16}$); 573 ($1.5\ 10^{16}$); 673 ($1.5\ 10^{16}$)
	Kr 500keV	298 (10^{16})
3% Fe	Thermal run (no irradiation)	[423 – 823]
	Ar 600 keV	298 ($7\ 10^{15}$), 573 ($1.5\ 10^{16}$)
	Kr 600 keV	573 (10^{16})
4.4% Fe	Ar 600 keV	573 (10^{16})
	Kr 500 keV	20 (10^{16}); 423 (10^{16})
	Kr 600 keV	423 ($5\ 10^{15}$)
5% Fe (nominal composition)	Kr 500 keV	298 ($5\ 10^{1)}$)

These experiments were conducted during four one-week trips to the Argonne facility, using the funds in the program. Use of the IVEM microscope was furnished free of charge to the program upon acceptance of a peer evaluated research proposal.

3.2 Phase Transformation during Thermal Annealing of thin films

The as-fabricated films show only the rings associated with hcp Zr (Figure 11a) indicating that the Fe is in solid solution in the Zr. The thermal runs show that new rings appear on the diffraction patterns after annealing at temperatures above 420-450°C. Figure 11b shows the rings present, including new rings indicated by arrows, after annealing at temperatures up to 550 C. These new rings are identified as the body centered tetragonal Zr_2Fe phase. This Zr_2Fe phase, although not the most stable thermodynamically, is often observed in melts of compositions where the orthorhombic Zr_3Fe phase (most stable thermodynamically) would be expected to be observed due to sluggishness in the formation of this last. At lower temperatures no change in the films was observed during the experiment.

The film showed grain coarsening as the temperature and/or experimental time was increased. The precipitation from the supersaturated solid solution results from classical homogeneous nucleation and thermal diffusion processes.

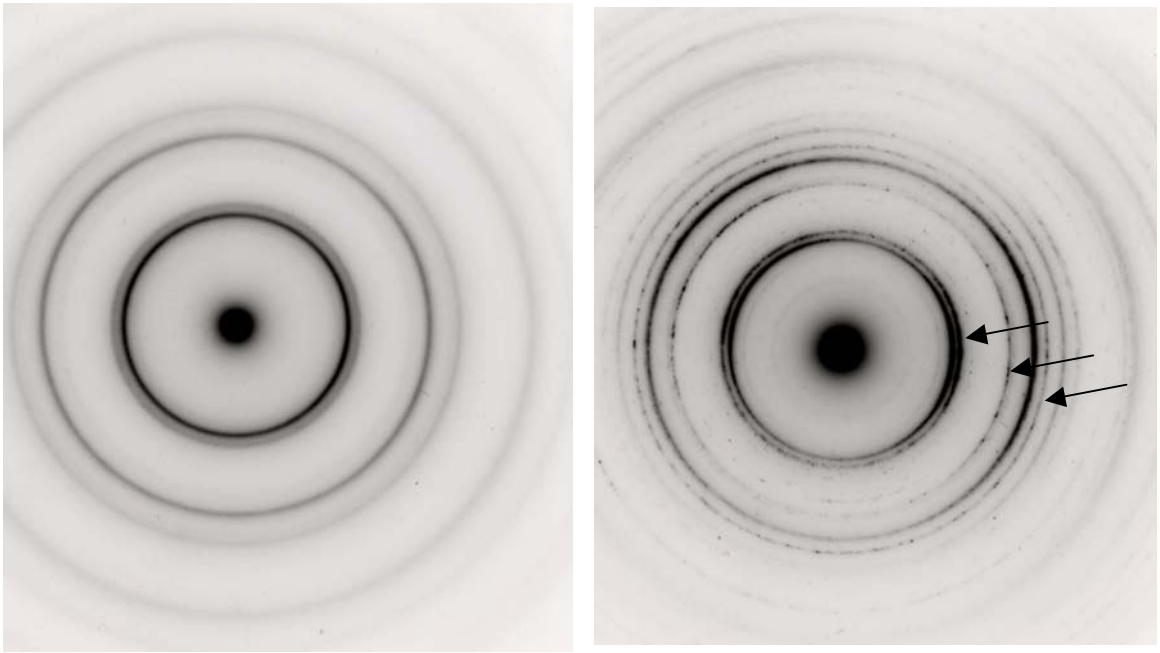

Figure11: Thermal effect on the supersaturated (Zr-3%Fe) film. On the left is the DP at room temperature (initial state); on the right the diffraction pattern was taken at 550 °C. The arrows indicate rings associated with new phase formation during irradiation.

3.3 Irradiation Induced Precipitation (IIP)

The in-situ ion irradiation of the Zr-Fe thin films showed the acceleration of the Zr_2Fe second phase precipitation, to varying degrees, depending on the specific irradiation conditions.

Figure 12 shows both electron micrographs (bright field and dark field images – BF/DF) and diffraction patterns obtained during in-situ Kr ion irradiation at 300 C. The region on the right was shadowed from the beam by a specimen grid and is therefore unirradiated; that on the left was irradiated to 10^{16} ion/cm^2 Kr ions. The diffraction pattern associated with the unirradiated region shows only the lines associated with the hcp phase, while the pattern from the irradiated region show the new lines from the irradiation induced precipitates shown in the micrographs. The right hand side of Figure 12 shows a dark field from one of the precipitate spots showing the presence of irradiation-induced precipitation in the region exposed to the beam.

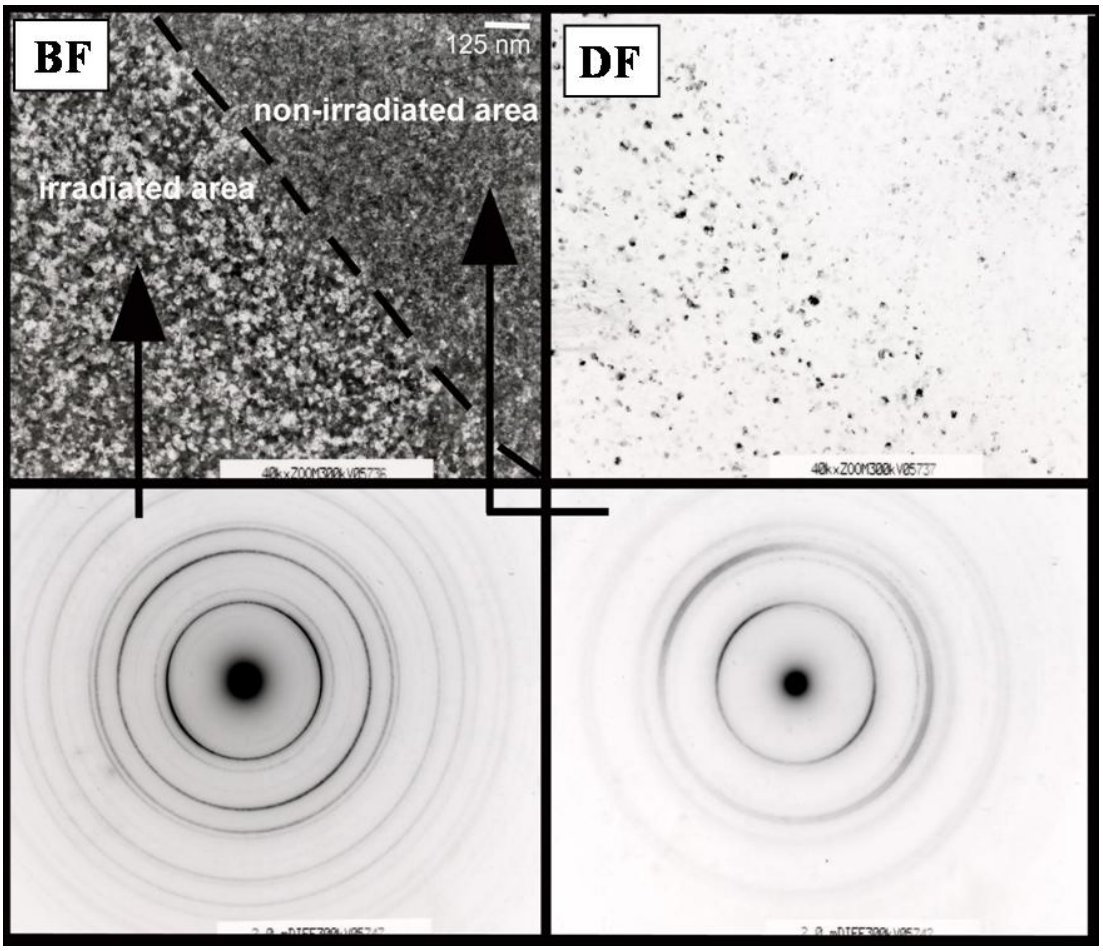

Figure 12: Irradiation induced precipitation (IIP) in Zr-Fe thin films studied in-situ in the electron microscope. One region is exposed to the Kr beam and exhibits precipitation after irradiation while the unexposed region still shows only the diffraction lines associated with hcp-Zr.

An initial attempt to quantify this precipitation is shown in Figure 13. The influence of temperature is to diminish the minimum dose to reaction during irradiation of Zr1.2%Fe thin films with 600 keV Kr ions. IIP increases with ion fluence, irradiation temperature and with ion mass (more precipitation with Kr than with Ar). The kinetics of the irradiation-enhanced precipitation can be characterized by the level of ion fluence at which the DPs first show the extra rings. This level clearly depends on the

temperature at which the irradiation is performed (thermo-irradiation combined effect), the composition of the film, and the type of ion. At a given temperature, samples of higher Fe concentration show reaction at lower ion fluences. As expected the ion type appears to have played a role in the kinetics of the reaction: at given sample composition and irradiation temperature, the first signs of reaction occur at a lower ion fluence for Kr (heavier ion) than Ar.

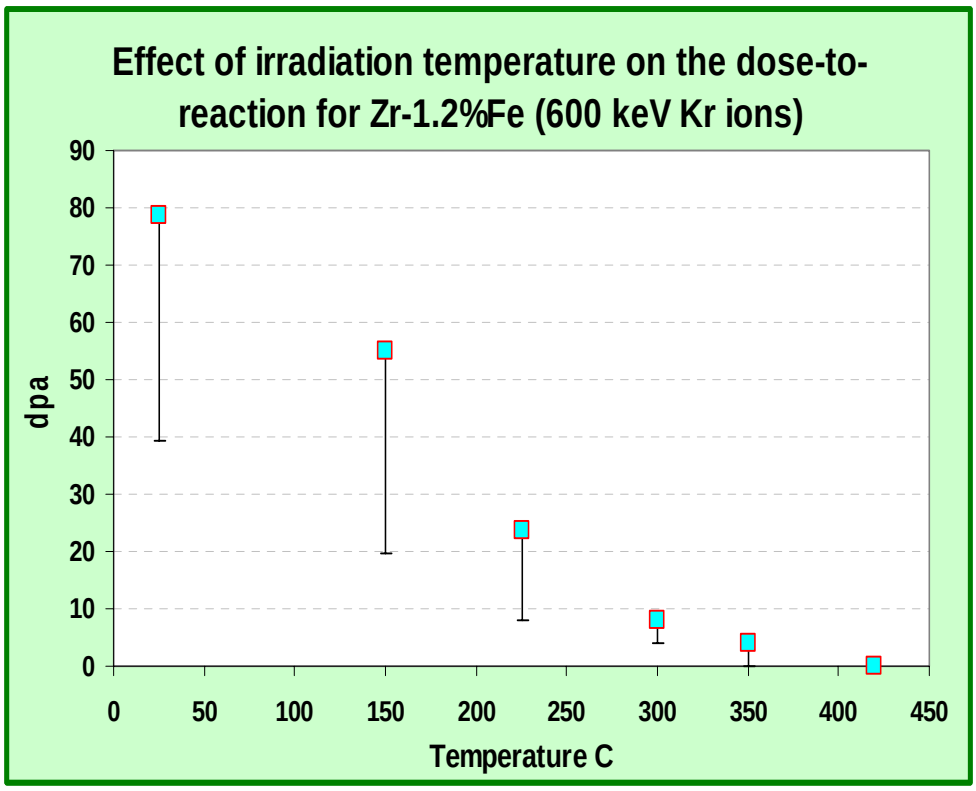

Figure 13: Dose in dpa for start of Zr_2Fe precipitation in ZrFe thin films during in-situ irradiation with Kr ions as function of irradiation temperature.

4. Irradiation Induced Grain Growth during In-situ irradiation (D. Kaoumi, A. Motta and in collaboration with Dr, Robert Birtcher at Argonne National laboratory)

During the same experiments that led to the precipitation and dissolution of second phases, we also observed the growth of the grains in the sample. A systematic study was then undertaken to develop an understanding of the grain growth process under irradiation.

The as-deposited thin film is shown in Figure 14. *In situ* ion beam irradiation was used to study irradiation-induced grain growth on co-sputter deposited Zr-xFe ($0 \leq x \leq 4.5\%$) nanocrystalline thin films. Samples were irradiated with Kr and Ar ions to fluences in excess of 10^{16} ions/cm^2, at irradiation temperatures ranging from 20K to 573K. The average grain size increased monotonically with ion fluence until it reached a saturation value. The grain growth at 20 K is similar to that which occurs at 298 K. Above this temperature range the grain growth increases with irradiation temperature.

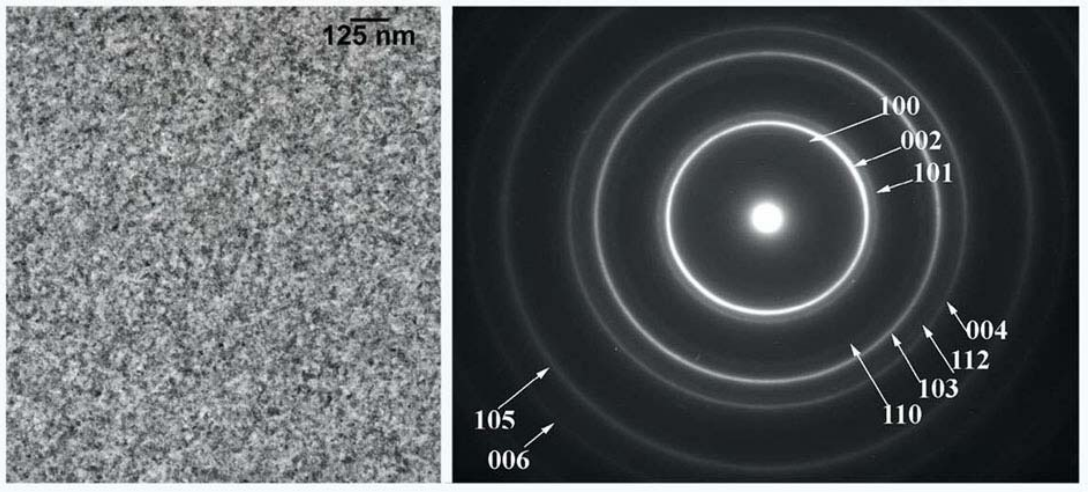

Figure 14: As-deposited thin film showing bright field image (left) and diffraction pattern showing only the hcp-Zr phase (right).

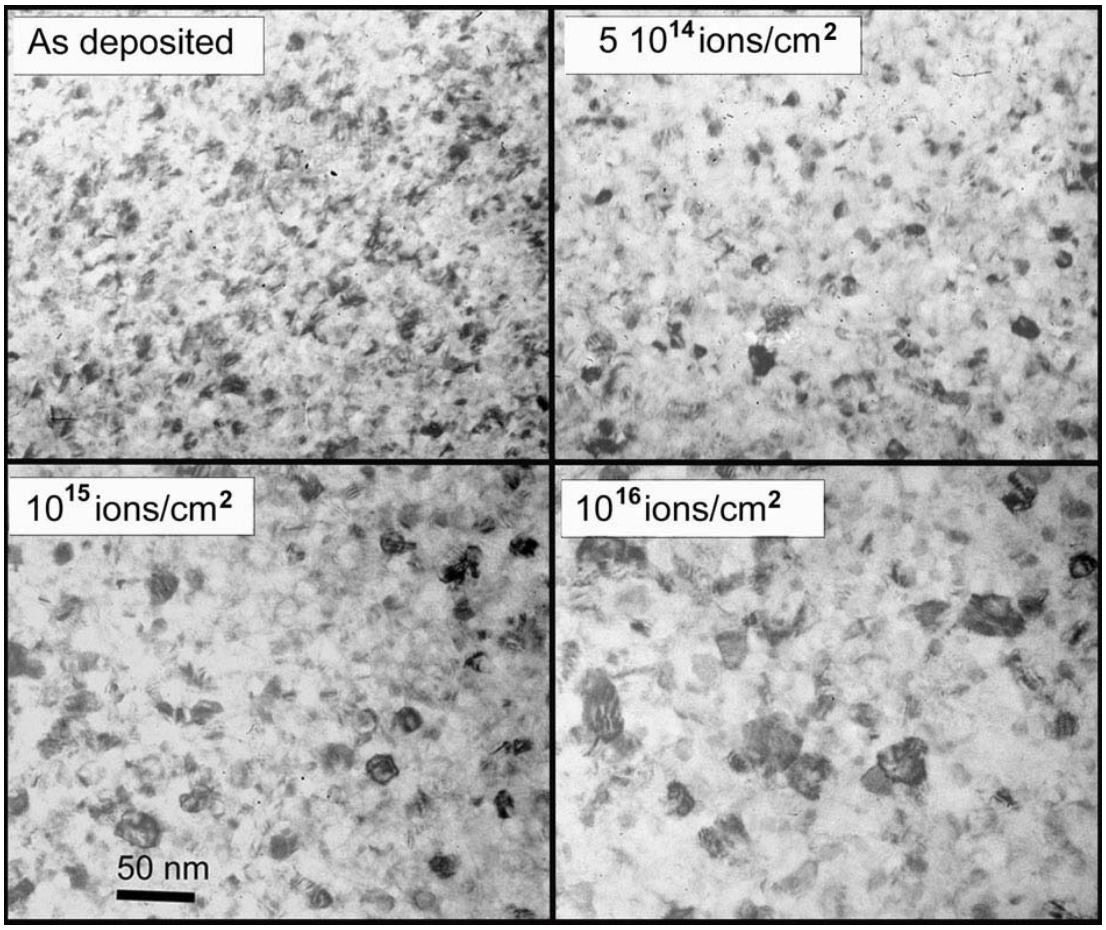

Figure 15: Bright Field sequence showing grain growth during ion irradiation in Zr film at 20 K as a function of ion fluence.

Direct observation of the films under irradiation revealed a gradual increase of the average grain size (i.e. average grain diameter), for all ion energies, at all irradiation temperatures, even at 20K where thermal effects are negligible. Figure 15 shows a sequence of bright field pictures of a pure zirconium film irradiated with 500 keV Kr^+ ions at 20K taken at different ion fluences. The increase of grain size is apparent on the micrographs and it could also be noted on the diffraction patterns which became spottier as the fluence increased, indicating grain size increase.

Figure 16 shows the evolution of the grain size distribution with ion fluence for Zr-4.4%Fe irradiated with Kr^+ ions at 20K. As the ion dose increases, the peak of the distribution shifts to larger average grain sizes. The evolution of the measured grain sizes with fluence is shown in Figure 15. For all compositions considered and all irradiating temperatures, grain size increases gradually and monotonically with ion dose until it reaches saturation. It is not clear what limits grain growth in this case. Possibilities are a solute effect, a cascade size effect, and the thickness of the thin foil. Similarly to thermal grain growth, these curves could be fitted with exponential curves of the type: $L^n - L_0^n = K\Phi$ where L_0 is the initial mean grain diameter Φ is the ion dose, K is a constant, and $2.5 \leq n \leq 4.5$. The grain size was calculated by taking the average of the smaller diameter and the larger diameter measured on the TEM micrographs.

We actually can distinguish two regimes of grain growth depending on the range of fluences (or grain sizes). Indeed the rate (i.e. K and n terms) seems to depend on the grain size (hence fluence). For small fluences (hence small grain sizes) grain growth is linear with respect to the fluence. The curves can be better fitted with straight lines (n=1). Once a critical fluence (corresponding to a critical average size) is reached grain growth slows down resulting in smaller rates (n>1); this happens around 2 to 3 10^{15} ions/cm^2. It is possible that the drag effect that finally slows the grain growth process leading to final grain size saturation, is overcome at small fluences by a higher grain-growth driving force due to the very fine grain size distributions.

The data in Figure 16 shows that the kinetics of ion-beam induced grain growth kinetics appear to be independent of temperature in the range below room temperature. There is little difference in the curves obtained at 20 K and at 293 K, suggesting that in this temperature range ballistic effects of ion irradiation dominate the grain growth process. At higher temperatures, the rate of grain growth and the final saturation grain size increase with temperature. Grain growth is a result of the combined effects of irradiation and temperature, and thermal processes likely become active at this temperature range.

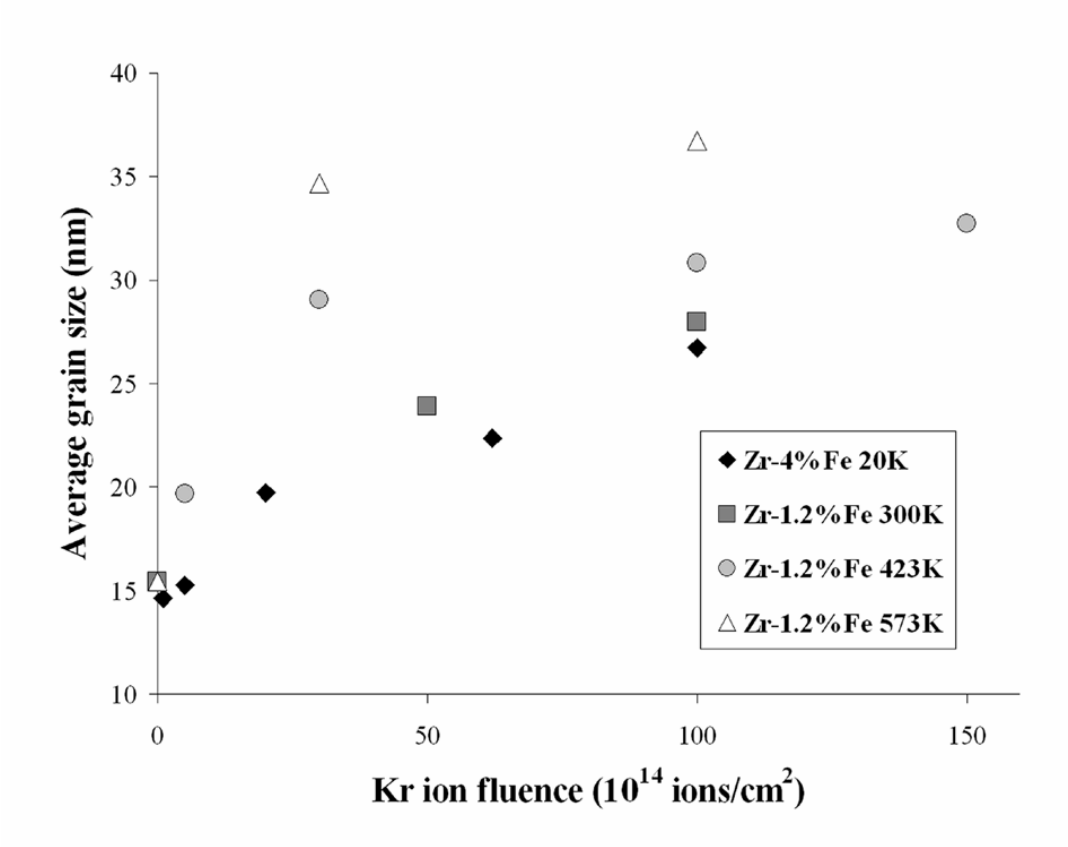

Figure 16: Average grain diameter versus ion fluence for several irradiation conditions.

5. Electron Irradiation of Zr-Fe thin films (D. Kaoumi, A. Motta and in collaboration with Dr. Isabelle Monnet at CEA-Saclay)

To investigate the role of displacement cascades and localization of damage on the formation of second phases during these experiments we performed limited experiments using electron irradiation using the high voltage electron microscope at the CEA-Centre d'Etudes Nucleaires de Saclay in France. For that purpose, D. Kaoumi went to the CEA laboratory at Saclay and spent two months as a student researcher while the PI was spending a sabbatical in the laboratory mentioned.

Thin films similar to those irradiated with ions were irradiated with high energy electrons to levels of damage above and beyond the levels obtained with ions. After several irradiations at temperatures ranging from room temperature to 450°C, no effect was observed of electron irradiation in enhancing the formation of Zr_2Fe precipitation, compared with the results obtained in the study of the effect of ion irradiation on the phase stability of the Zr-Fe thin films done previously. The results indicate that electron irradiation induces some grain coarsening and the formation of a new phase most likely to be identified as an oxide resulting from imperfect vacuum in the microscope. The experiments at high temperature (450°C) showed clearly some intermetallic formation, but because this occurred in the non-irradiated regions of the sample as well, this high temperature formation of compounds is purely a thermal effect.

6. Conclusions

Extensive work was performed both in synchrotron radiation x-ray diffraction examination of precipitates microstructure in Zr alloys and on in-situ irradiation of ZrFe thin films to obtain data on the precipitation behavior of these alloys and overall influence of alloying elements on microstructure evolution.

1. The examination of model alloys at different stages of annealing with synchrotron radiation sources indicates that such examinations can provide a very accurate picture of the bulk state of precipitation in the material such that quantification of the precipitation can be attempted. Such techniques can be applied to neutron irradiated samples if appropriate safety measures are taken to handle radioactive materials.
2. The co-deposition of thin films of Zr and Fe on soluble substrates creates metastable supersaturated solid solutions which can then be used as a model system to study in detail alloy evolution.
3. The in-situ irradiation experiments performed at temperatures from 30 to 600 K showed that new intermetallic phases formed in the alloy as a result of being exposed to irradiation. This irradiation induced precipitation increased with fluence, temperature and with ion mass for a given fluence.
4. Ion irradiation induced grain growth of hcp Zr grains was also observed in situ and some main points are salient: the results presented here indicate that grain growth occurs for all the irradiation temperature studied. Grain growth was similar at 20 K and 298 K, and increased with irradiation temperature above 298 K, indicating a lower temperature regime controlled by collisional processes and a higher temperature regime where thermally activated processes increase the rate of grain growth.

7. References:

1. D. Kaoumi, A. Motta, I. Monnet, J. Perinet, T. Van den Berghe, “Study of the effect of 1 MeV electron irradiation on Zr thin films supersaturated with Fe”, CEA-Saclay, Report number CR-SRMA-03-1683, 2003.
2. D. Kaoumi, A. T. Motta, R. C. Birtcher, “Grain Growth in Metallic Thin Films during In Situ Ion Irradiation in a TEM,” submitted to Nuclear Instruments and Methods in Physics Research, August, 2004.
3. S. Jurgensmeier, Y.Chu, A.T.Motta, “Precipitates in Zirconium Alloys Studied using Synchrotron Radiation”, to be submitted to the Journal of Nuclear Materials, 2004.
4. D. Kaoumi, A. Motta, R. Birtcher, “Microstructure Evolution in Zr-Fe Thin Films During In-situ Ion Irradiation in a TEM”, presentation at the 14th Ion Beam Modification of Materials , September 2004.
5. D. Kaoumi, A. Motta, R. Birtcher, “Phase Formtion During Ins-tu irradiation on Zr-Fe thin films”, in preparation for submission to Journal of Applied Physics, 2004.
6. D. Kaoumi, A. Motta, R. Birtcher, “Influence of Temperature and ion type on irradiation induced grain growth in thin films, in preparation for submission to the Journal of Nuclear Materials, 2004.

8. Graduate Student theses generated during the project at Penn State

Sarah Jurgensmeier; M.Sc. thesis in Materials, December 2002
"Identification of Second Phases in Zirconium Alloys"

Djamel Kaoumi, Ph.D Thesis; envisaged December 2005
"Irradiation Induced Microstructure Evolution in Zirconium Alloy thin films"